Parity–time-symmetric photonic topological insulator

Check for updates

Alexander Fritzsche[1,2], Tobias Biesenthal[1], Lukas J. Maczewsky [1], Karo Becker [1], Max Ehrhardt [1], Matthias Heinrich [1], Ronny Thomale [2], Yogesh N. Joglekar [3] ✉ & Alexander Szameit [1,4] ✉

Topological insulators are a concept that originally stems from condensed matter physics. As a corollary to their hallmark protected edge transport, the conventional understanding of such systems holds that they are intrinsically closed, that is, that they are assumed to be entirely isolated from the surrounding world. Here, by demonstrating a parity–time-symmetric topological insulator, we show that topological transport exists beyond these constraints. Implemented on a photonic platform, our non-Hermitian topological system harnesses the complex interplay between a discrete coupling protocol and judiciously placed losses and, as such, inherently constitutes an open system. Nevertheless, even though energy conservation is violated, our system exhibits an entirely real eigenvalue spectrum as well as chiral edge transport. Along these lines, this work enables the study of the dynamical properties of topological matter in open systems without the instability arising from complex spectra. Thus, it may inspire the development of compact active devices that harness topological features on-demand.

The discovery of the quantum Hall effect[1] shed the first light on the role of topology in correlated electron systems, and thereby inspired the subsequent emergence of topological insulators[2–6] as one of the most active current areas of research across a variety of fields in physics. As an independent class of materials in their own right, these systems are characterized by topologically protected transport along their boundary that is robust against defects and disorder. By contrast, their bulk typically remains entirely insulating or features substantially reduced rates of wave packet diffraction. In recent years, topological insulators have been experimentally realized and studied on a wide range of different physical platforms[7–14]. All of these implementations, however, have Hermiticity in common, as they inherently assume closed systems, and their dynamics can therefore be described entirely independently of global attenuation or amplification. Yet, non-Hermiticities are omnipresent in realistic physical systems due to interactions with the environment. Although the energy exchange associated with such coupling to a reservoir in general gives rise to exponentially decaying or amplified states, certain symmetries may keep such instability at bay: as was shown by Bender and Böttcher in 1998, parity–time-symmetric (PT-symmetric)[15] configurations can globally exhibit real eigenvalue spectra despite featuring a non-zero imaginary part of the potential landscape. As it turns out, these properties are not restricted to a combination of parity flip and time reversal, but can in fact be generalized to all self-inverse antiunitary operators[16]. The notion of PT symmetry encountered particularly fertile ground in photonics, where the imaginary part of potentials can be readily implemented as gain and loss for electromagnetic waves. In conjunction with the refractive index that represents the potential's real part, light-based settings enabled the experimental exploration of PT-symmetric systems and their peculiar features, ranging from non-orthogonal eigenmodes to the emergence of exceptional points[17–24] at the phase transition that marks the spontaneous breaking of this complex symmetry. More recently, efforts to combine the two previously separate realms of topology and non-Hermiticity have resulted in an extensive topological classification

[1]Institute of Physics, University of Rostock, Rostock, Germany. [2]Institut für Theoretische Physik und Astrophysik, Julius-Maximilians-Universität Würzburg, Am Hubland, Würzburg, Germany. [3]Department of Physics, Indiana University–Purdue University Indianapolis (IUPUI), Indianapolis, IN, USA. [4]Department of Life, Light and Matter, University of Rostock, Rostock, Germany. ✉e-mail: yojoglek@iupui.edu; alexander.szameit@uni-rostock.de

of non-Hermitian symmetries[25] as well as important advances ranging from topological insulator lasers[26] and their acoustic counterparts[27] to light steering along interfaces between dynamically defined amplifying and attenuating domains[28], topological funnelling of light[29] and the direct measurement of a non-Hermitian topological invariant[30]. Notably, although PT symmetry and topological insulators were at first considered to be mutually exclusive[31], subsequent experiments in one-dimensional photonic structures[32,33], electronic circuits[34] and mechanical metamaterials[35] nevertheless showed that non-trivial topological features can indeed be found in certain PT-symmetric arrangements, and even tuned by means of nonlinearity[36]. However, a key obstacle was found to be the selective breaking of the PT symmetry in chiral boundary states[37]. There are theoretical proposals at hand to overcome the issue[38,39]. However, they are based on requirements that are challenging to implement on integrated-optical platforms, such as non-Hermitian hopping terms or precisely tuned continuous spatiotemporal gain–loss distributions. As a result, the experimental realization of a genuine PT-symmetric topological insulator remains elusive to this day.

In this work, we theoretically propose and experimentally demonstrate a non-Hermitian topological insulator with an entirely real spectrum. In contrast to conventional static implementations of PT symmetry that arrange gain and loss spatially[23–35], we construct a periodically driven Floquet model that distributes the non-Hermitian components dynamically in both space and time (compare with Fig. 1). In particular, we employ a generalized PT-symmetric extension of a $\mathbb{Z}_2$ topological insulator[40] and implement the constituent steps of its anomalous Floquet driving protocol[41–44] in a mesh-like arrangement of selectively coupled optical wave guides. This approach allows us to overcome the limitations discussed in the literature[31] and realize a system with a novel type of topological boundary states. Notably, in this dynamical non-Hermitian arrangement, the system's bulk as well as edge states are protected from instability that would typically be induced by coupling to the environment and preclude a lasting transport along the edge, as evidenced by the fact that the quasi-energy band structure remains entirely independent of it (Supplementary Section 2).

In the tight-binding limit, light evolves in our two-dimensional photonic structure in accordance with the discretized paraxial Helmholtz equation (Supplementary Section 1):

$$\mathrm{i}\frac{\mathrm{d}}{\mathrm{d}z}E_m(z) = g_m(z)E_m(z) + \sum_{l\in\langle m\rangle}c_{l,m}(z)E_l(z) \tag{1}$$

for the electric field amplitude E_j at lattice site j. It is formally equivalent to the Schrödinger equation with the third spatial dimension z playing the role of time[45], which is why, in the following, we will refer to z as time. The transverse dynamics are represented by the sum over the nearest neighbours $\langle m\rangle$ of site m. The driving protocol itself is periodic along z with a Floquet period of L, and the on-site potentials $g_m(z)$ are piecewise constant for six discrete steps of equal length $L/6$. Similarly periodic Hermitian couplings $c_{l,m}(z)$ are chosen such that, in each step, only specific pairs of nearest neighbours interact (Fig. 2). The full dynamics of the system are therefore described by the Floquet operator after one period:

$$U(L) = U_6U_5U_4U_3U_2U_1 = \mathrm{e}^{-\mathrm{i}H_\mathrm{eff}L} \tag{2}$$

with the effective Hamiltonian H_eff and $U_n = \mathrm{e}^{-\mathrm{i}H_nL/6}$ with the (static) single-step Hamiltonians H_n. The explicit forms of these operators are provided in Supplementary Tables 1 and 2. The eigenvalues $\mathrm{e}^{-\mathrm{i}\varepsilon L}$ of the Floquet operator yield the quasi-energies ε that, due to the cyclic driving protocol, are periodic[43] with $2\pi/L$. For real-valued on-site potentials $g_m(z)$, the Floquet operator is by definition unitary, and the effective Hamiltonian (compare with equation (2)) is Hermitian $H_\mathrm{eff}^* = H_\mathrm{eff}^\mathrm{T}$, where
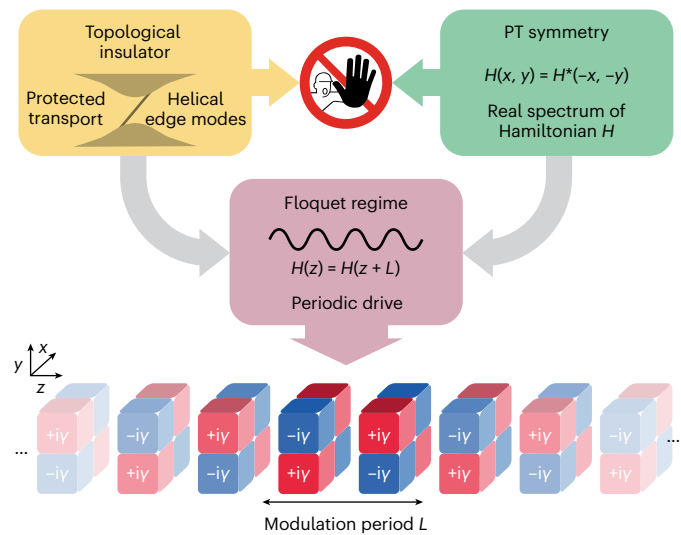

Fig. 1 | Conceptual idea of a PT-symmetric topological insulator. Conventional wisdom regards topological insulators and PT symmetry as mutually exclusive concepts. Distributing gain and loss ($\pm\mathrm{i}\gamma$, indicated as red (+) and blue (−), respectively) dynamically along the spatial degrees of freedom x and y and the evolution coordinate z of a periodically modulated system allows for the construction of a complex Floquet drive that overcomes this dichotomy by simultaneously supporting topologically protected edge transport and an entirely real eigenvalue spectrum in a genuinely non-Hermitian arrangement.

* denotes complex conjugation and T denotes transposition. Similar to the model discussed in the literature[46,47], the unit cell of our lattice comprises a total of four sites belonging to two distinct sublattices (indicated in Fig. 2a as black for sublattice A and white for sublattice B). Note that while inter-sublattice couplings are crucial for the desired photonic $\mathbb{Z}_2$ topological insulator[40] to be established, they are confined to steps 2 and 5, while all remaining steps exclusively promote interactions within each of the two sublattices. In this vein, the protocol gives rise to a pair of counter-propagating boundary states that are topologically protected by virtue of fermionic time reversal symmetry defined by

$$\mathcal{T}H^*(z)\mathcal{T}^{-1} = H(L-z), \tag{3}$$

where $\mathcal{T}(\mathcal{T}^{-1})$ denotes the (inverse) time reversal operator and fulfils $\mathcal{T}\mathcal{T}^* = -\mathbb{1}$.

To extend this Hermitian Floquet system in a PT-symmetric fashion, we introduce complex on-site potentials $g(z) \to \pm\mathrm{i}\gamma(z)$ whose imaginary part $\pm\gamma$ encodes gain (+) as well as loss (−) with equal magnitudes. As a result, the system's Hamiltonian is no longer Hermitian, that is $H^* \neq H^\mathrm{T}$, and as such allows for two distinct variants of time reversal symmetry: the conventional one using complex conjugation (equation (3)), and a different one relying instead on transposition:

$$\mathcal{T}H^\mathrm{T}(z)\mathcal{T}^{-1} = H(L-z). \tag{4}$$

While both of these non-Hermitian symmetries can in principle support a pair of topologically protected boundary states[25], the transposition-based approach detailed in equation (4) readily allows for the non-Hermitian contributions to be placed in coupling steps 1, 3, 4 and 6 (Fig. 2a) where only intra-sublattice couplings occur. Such an alternating and step-wise balanced arrangement ensures that whenever one of the sublattices experiences gain, the other one is subject to loss (Fig. 2a). Importantly, despite the genuinely non-Hermitian single-step Hamiltonians and the accordingly non-unitary Floquet operator, the quasi-energy spectrum of both the bulk and the

boundary states remains entirely real for arbitrary values of γ (Fig. 2b). This is a direct result of the connection of the non-unitary Floquet operator $U(\gamma \neq 0, L)$ to its unitary counterpart $U(\gamma = 0, L)$, which can be written as $U(\gamma = 0, L) = M(\gamma)U(\gamma, L)M^{-1}(\gamma)$, with $M(\gamma) = \text{Diag}(\exp(2\gamma), 1, \exp(2\gamma), 1)$, in line with the time reversal symmetry and the temporal distribution of the gain and loss. Consequently, the non-Hermitian system strictly retains both the real eigenvalue spectrum and the topological properties of the Hermitian case, despite undergoing an unequivocally non-unitary time evolution that distinguishes it from its Hermitian counterpart[40]. In other words, the proposed arrangement has only an unbroken PT-symmetric phase regardless of the applied contrast between gain and loss. A detailed analysis of the properties of the Floquet operator and the generalized PT symmetry of the effective Hamiltonian is provided in Supplementary Section 2. Due to the non-orthogonality of the eigenstates of the Floquet operator, the intensity of any given state is no longer a conserved quantity but rather oscillates along z (Supplementary Section 4 and Supplementary Fig. 3)—a well-known and crucial dynamical feature of PT-symmetric systems[17].

To experimentally probe the topological transport characteristics of our system, we employed the femtosecond laser direct writing technique[48] to fabricate wave guide lattices composed of 4×3 unit cells in the transverse (x, y) plane and two full Floquet cycles along z in a 150-mm-long fused silica sample. In each step of the driving protocol, the respectively interacting wave guides are brought into close proximity to one another via sinusoidal bends so as to facilitate the desired fraction of light to be transferred between them while suppressing interactions between all other lattice sites[43]. Along these lines, the four intra-sublattice couplings (steps 1, 3, 4 and 6) are set to fully transfer light from one wave guide to the next to ensure a maximum degree of helicity. By contrast, the couplers for steps 2 and 5 have to be designed for a fractional transfer between the sublattices, as perfect coupling (or full transfer of light) in these components would render the Floquet operator trivially unitary (Supplementary Section 3). Along these lines, an inter-sublattice transfer ratio of $(67.8 \pm 0.75)\%$ was implemented in the experiments. In turn, the non-Hermitian features of the system were established by introducing losses via a multiplicity of microscopic scattering centres deliberately created during the inscription process[23]. These microscopic points scatter some light away from the wave guide such that it is effectively lost to the environment. In this fashion, we systematically shifted the imaginary part of the spectrum to allow for an entirely gain-free or passive implementation that faithfully reproduces the PT-symmetric characteristics of the gain/loss arrangement while avoiding the thermal noise associated with net-gain regions[49]. Note that steps 2 and 5 are realized without additional losses, and, in the co-moving dampened frame, this corresponds to an effective gain. This absence of true gain faithfully preserves the characteristic dynamics of the system while allowing for an entirely passive experimental implementation. The distribution of the lossy sections within one Floquet unit cell of the wave guide mesh is highlighted in Fig. 3a. In the fabricated wave guide lattice, each of these lossy sections reduced the guided intensity by $(17.7 \pm 0.4)\%$.

In a first set of measurements, we investigated the light propagation in the interior of the lattice. When any individual site of an internal unit cell is excited, the injected laser beam undergoes pronounced omnidirectional spreading regardless of the targeted sublattice (Fig. 3b), as bulk transport would be suppressed only for perfect inter-sublattice transfer (Supplementary Section 4). By contrast, for our second set of measurements, single-site excitations were placed along the circumference of the array to populate the system's helical edge states. Notably, as shown in Fig. 4a,b, the specific choice of the excited sublattice determines the orientation of the transport (clockwise for sublattice A and counterclockwise for sublattice B). We trace the path of these channels by systematically moving the point of injection along the perimeter of the lattice. In either case, the respective topological
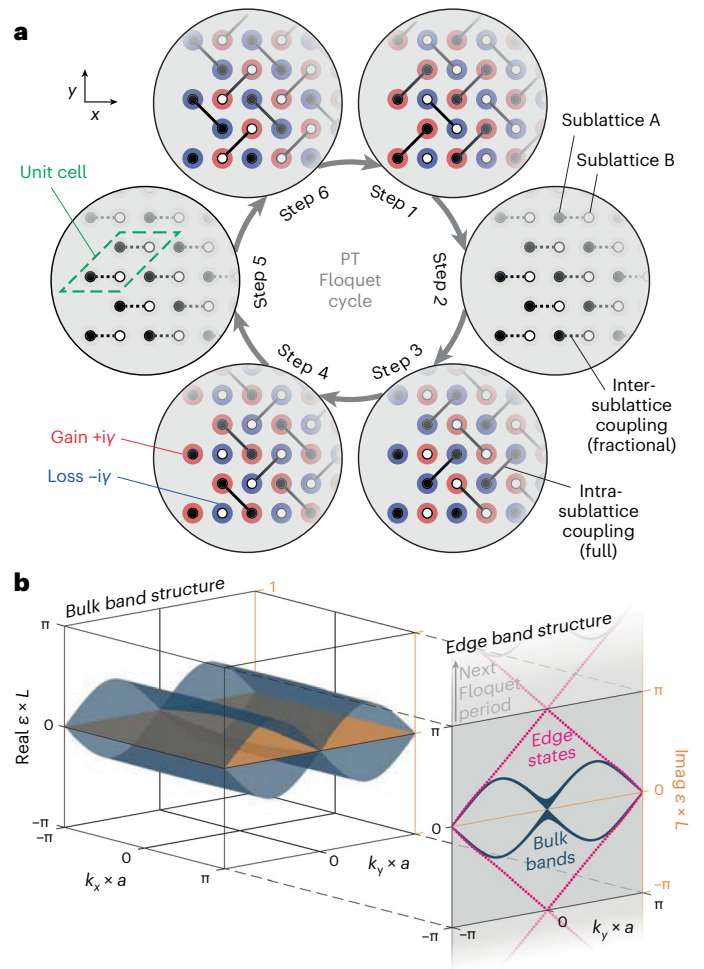
Fig. 2 | Non-Hermitian Floquet driving protocol and band structure. a, As a PT-symmetric generalization of the anomalous $\mathbb{Z}_2$ drive[40], our protocol consists of six distinct steps in which individual pairs of sites are allowed to interact. Note that only excitations in the two sites residing near the obtuse-angle (135°) corners of the rhombic unit cell (marked by a green dashed outline) populate the chiral edge states of the driven lattice, whereas excitations of the other two sites near the acute-angle (45°) corners result in closed loops. The individual sites of the two sublattices, A and B, are indicated by black and white-filled circles, respectively, while the presence of gain and loss is highlighted by red and blue haloes, respectively. **b**, The left side shows the numerically calculated bulk band structure as function of the quasimomenta k_x and k_y for full intra-sublattice coupling (solid connecting lines in steps 1, 3, 4 and 6 of **a**) and 66% inter-sublattice coupling (dashed connecting lines in steps 2 and 5 of **a**). Here, a denotes the lattice constant. The blue-shaded surface represents the real part of the quasi-energy ε. The intact PT symmetry of the arrangement is evidenced by the globally vanishing imaginary (Imag) part (orange). The right side shows that in addition to the projection of the bulk bands (blue), the edge band structure (numerically calculated for a semi-infinite ribbon) exhibits a pair of dispersion-free counter-propagating chiral edge states (dotted magenta lines) that likewise feature entirely real eigenvalues.

channel (indicated by dashed magenta outlines) is observed to flow along the edges and around the corners of the system. Note that both counter-propagating edge states are confined to the respective outermost rows of the lattice when propagating parallel to the x axis. By contrast, the 'bearded' edges defined by the arrangement of rhombic unit cells along the y axis lead to a spatial separation of the topological channels. As an illustration of this behaviour, we introduced a single-site defect in the lower right-hand corner of the fabricated wave guide array. Being located on the A sublattice, the clockwise-propagating edge state
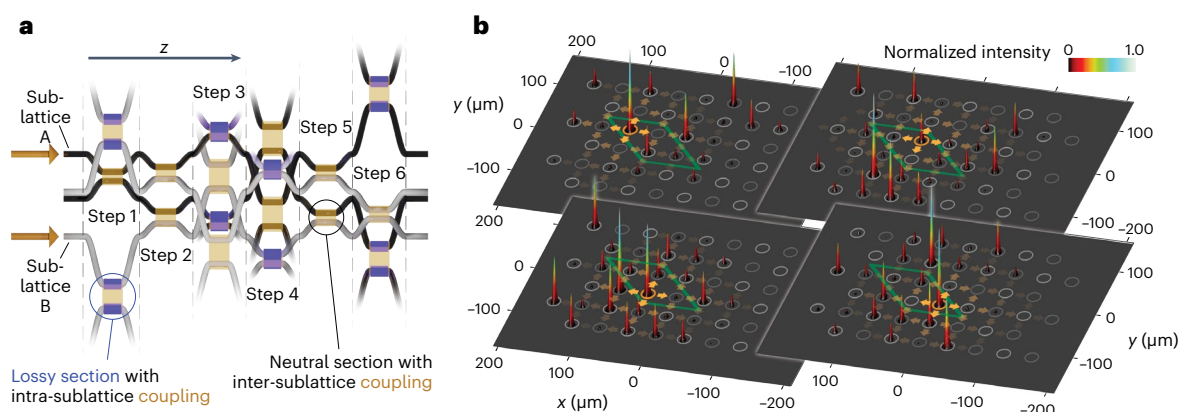
Fig. 3 | Photonic implementation and bulk excitations. a, Schematic of the three-dimensional wave guide mesh lattice that implements the proposed protocol in an entirely passive setting. Shown is one transverse unit cell as well as the sections of wave guides from the adjacent unit cells it interacts with in the course of the driving cycle. The sublattices A and B are indicated by the respective colours (dark/light grey) of the wave guides, and the regions with deliberately introduced losses are shaded purple. More details are provided in Supplementary Fig. 2. **b**, Experimentally observed intensity output patterns at the output facet of the sample resulting from single-site bulk excitations in a lattice composed of 3 × 4 unit cells. As a guide to the eye, positions of the wave guides of this lattice are indicated by grey circles, whereas the four different initially excited wave guides of a bulk unit cell (green rhombus) are highlighted with orange circles. Note that in each case, the wave packets are subject to substantial bulk diffraction (highlighted by the orange arrows) enabled by the fractional inter-sublattice couplings in steps 2 and 5 of the driving protocol. Simulations of the degree of bulk localization for different inter-sublattice couplings are provided in Supplementary Fig. 4.
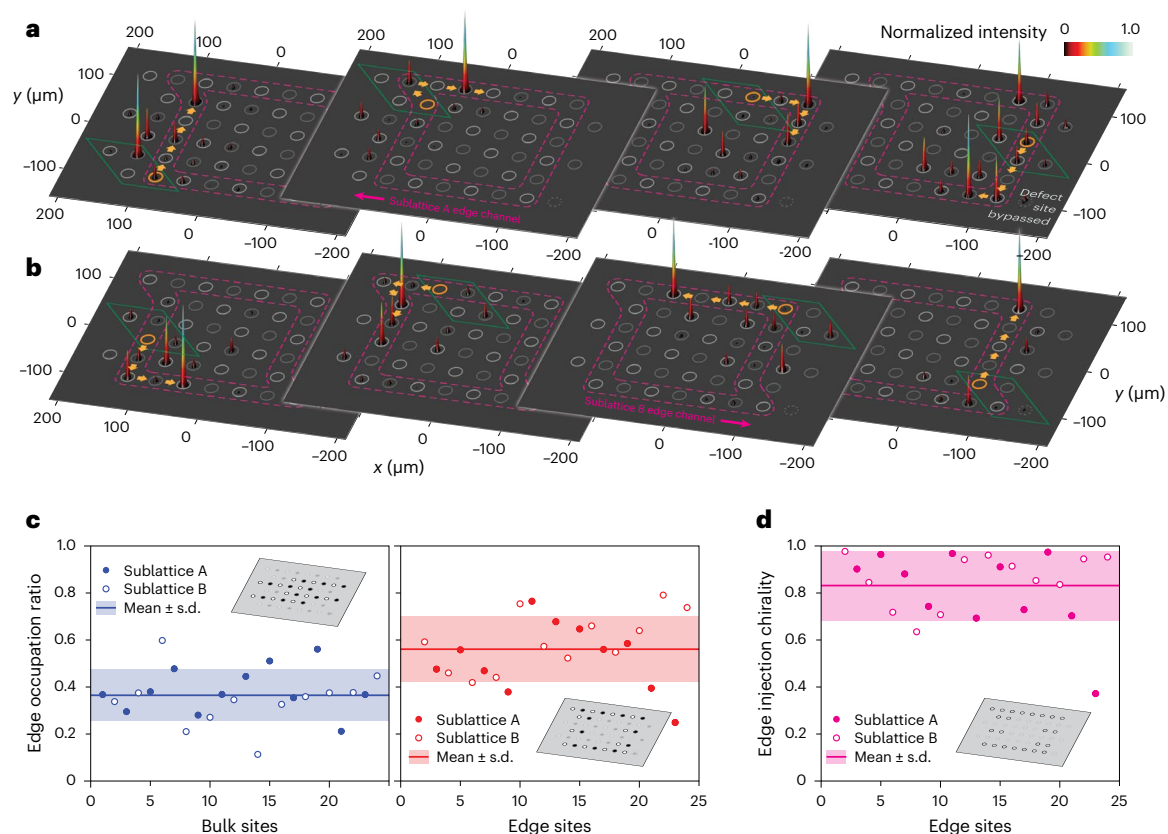

Fig. 4 | Counter-propagating topological edge states. a,b, Tracking the pair of counter-propagating topological edge channels associated with the two sublattices (dashed magenta outlines). Shown are the intensity distributions after two driving periods as observed at the output facet of the sample when injecting light into specific edge sites (highlighted in orange). Note that, while both channels flow along the outermost sites of the *x* edges (orange arrows), their paths are offset by half a unit cell (green rhombus) along the *y* edges. As a result, the clockwise-propagating channel of sublattice A shifts to bypass the deliberately induced defect in the lower right-hand corner (right panel of **a**), while the channel of sublattice B remains unaffected. **c**, EOR (fraction of the overall intensity contained in the edge channels) for a single-site edge (0.56 ± 0.03, right panel) and bulk excitations (0.36 ± 0.02, left panel). **d**, The chiral nature of topological transport in our system is clearly demonstrated by the ratio of 0.83 ± 0.03 between the intensities of the five leading versus trailing edge channel sites for each injection location evaluated for the entire set of edge excitations. The insets in **c** and **d** schematically indicate the bulk/edge excitation positions included in the analysis for the respective panels.

readily bypasses this defect (fourth panel in Fig. 4a) while the counter-clockwise channel of sublattice B remains unaffected.

To probe the detailed characteristics of the topological transport in our system in a quantitative manner, we evaluated the edge occupation ratio (EOR) as a fraction of the total output intensity observed in the appropriate edge channels (compare with Fig. 4c). While a certain amount of light injected into bulk sites inevitably reaches the edge unit cells due to the aforementioned residual bulk diffraction (left panel, $EOR_{bulk} = 0.36 \pm 0.02$), more than half of the light injected into the appropriate edge sites ends up in the topological channels (right panel, $EOR_{edge} = 0.56 \pm 0.03$). While EOR represents a measure of the injection efficiency of the edge states, the helical nature of these entities has to be taken into account to evaluate the specificity of the topological transport. To this end, we calculated the chirality χ as the ratio between the intensities contained within the five leading versus trailing edge channel sites (Fig. 4d). With a value of $\chi = 0.83 \pm 0.03$, this quantity unequivocally proves that our PT-symmetric Floquet drive indeed establishes a $\mathbb{Z}_2$-type anomalous topological insulator whose pair of protected edges remains highly directionally selective despite the underlying complex refractive index landscape of the arrangement. Note that the non-unity coupling in steps 2 and 5 (Fig. 2a), while necessary to establish non-trivial non-Hermitian conditions, results in a certain overlap of dispersive bulk bands with the edge sites of the lattice. As such, single-site excitations inevitably yield a certain population of bulk states. Upon injection, the light contained in those bulk states propagates through the interior of the finite lattice in a non-chiral fashion, and parts of it eventually deliver some intensity to the trailing wave guides of the excited boundary state, thereby preventing experiments in finite lattices from reaching a perfect EOR_{edge} and χ. This bulk state excitation could be reduced by applying a broad Gaussian light injection into the boundary sites that corresponds to a narrow Gaussian excitation in k-space, which would in turn allow a more precise targeting of the corresponding boundary mode. However, such an excitation of only the clockwise or counterclockwise moving state is difficult due to the sublattice structure of the underlying unit cell allowing only both states to be excited using this injection method.

A signature of the non-Hermiticity of the system is fluctuations of the overall intensity when spectrally broad wave packets are propagating. In particular, placing sublattice-specific single-site excitations results in different total intensities. This is in stark contrast to the Hermitian regime where the orthogonality of eigenstates fundamentally precludes such a difference. In our experiments, we indeed find that the intensities resulting from excitations on sublattice A on average exceed those placed on sublattice B by approximately $(19.4 \pm 2.5)\%$, in line with the numerical value of $(13.6 \pm 1.2)\%$ and substantially larger than the $(1.9 \pm 5.0)\%$ observed due to the slightly non-uniform injection efficiencies in the Hermitian reference system.

In conclusion, we have presented experimental evidence of the existence of a non-Hermitian topological insulator with a real-valued energy spectrum—an important missing link between the realms of topology and non-Hermiticity. In particular, the spatiotemporal distribution of gain and loss ensures that the generalized PT symmetry is protected against spontaneous symmetry breaking; that is, the arrangement remains pseudo-Hermitian regardless of the magnitude of the applied gain–loss contrast. The lattice design allows for the two counter-propagating topological channels to be spatially separated along the 'bearded'-type edge. We have shown that this chiral transport is robust against single-site defects, which are circumnavigated in a sublattice-specific fashion, underlining the topological nature of our system, which can be extended to all PT-symmetric topological insulators. Interestingly, our approach allows us to interpret the evolution direction as a third spatial dimension instead of as a temporal one[50], permitting the experimental investigation of the impact of non-Hermiticities on topological singularities in higher-dimensional systems. Furthermore, while our experiments were conducted on a photonic set-up, the underlying non-Hermitian Floquet protocol can readily be generalized to any platform that allows for the implementation of discrete coupling steps and dynamic control of loss or gain, ranging from topological acoustics[51] to topolectrical circuits[52]. Along these lines, the rich interplay between complex modulation and topology in open systems is brought into the reach of future experiments by the robust nature of the topological PT-symmetric Floquet protocol presented here, providing a pathway to exploit the dynamical properties of non-Hermitian topological systems without the instabilities entailed by complex spectra.

Online content

Any methods, additional references, Nature Portfolio reporting summaries, source data, extended data, supplementary information, acknowledgements, peer review information; details of author contributions and competing interests; and statements of data and code availability are available at https://doi.org/10.1038/s41563-023-01773-0.

References

1. Klitzing, K. V., Dorda, G. & Pepper, M. New method for high-accuracy determination of the fine-structure constant based on quantized Hall resistance. *Phys. Rev. Lett.* **45**, 494–497 (1980).
2. Kane, C. L. & Mele, E. J. Z_2 topological order and the quantum spin Hall effect. *Phys. Rev. Lett.* **95**, 146802 (2005).
3. Bernevig, B. A. & Zhang, S. C. Quantum spin Hall effect. *Phys. Rev. Lett.* **96**, 106802 (2006).
4. König, M. et al. Quantum spin Hall insulator state in HgTe quantum wells. *Science* **318**, 766–770 (2007).
5. Haldane, F. D. M. Model for a quantum Hall effect without Landau levels: condensed-matter realization of the 'parity anomaly'. *Phys. Rev. Lett.* **61**, 2015–2018 (1988).
6. Hasan, M. Z. & Kane, C. L. Colloquium: topological insulators. *Rev. Mod. Phys.* **82**, 3045–3067 (2010).
7. Klembt, S. et al. Exciton-polariton topological insulator. *Nature* **562**, 552–556 (2018).
8. Hoffmann, T. et al. Chiral voltage propagation and calibration in a topolectrical Chern circuit. *Phys. Rev. Lett.* **122**, 247702 (2019).
9. Süsstrunk, R. & Huber, S. D. Observation of phononic helical edge states in a mechanical topological insulator. *Science* **349**, 47–50 (2015).
10. Wang, Z., Chong, Y., Joannopoulos, J. D. & Soljačić, M. Observation of unidirectional backscattering-immune topological electromagnetic states. *Nature* **461**, 772–775 (2009).
11. Rechtsman, M. C. et al. Photonic Floquet topological insulators. *Nature* **496**, 196–200 (2013).
12. Hafezi, M., Demler, E. A., Lukin, M. D. & Taylor, J. M. Robust optical delay lines with topological protection. *Nat. Phys.* **7**, 907–912 (2011).
13. Lu, L., Joannopoulos, J. D. & Soljačić, M. Topological photonics. *Nat. Photon.* **8**, 821–829 (2014).
14. Ozawa, T. et al. Topological photonics. *Rev. Mod. Phys.* **91**, 015006 (2019).
15. Bender, C. M. & Boettcher, S. Real spectra in non-Hermitian Hamiltonians having PT symmetry. *Phys. Rev. Lett.* **80**, 5243–5246 (1998).
16. Bender, C. M., Berry, M. V. & Mandilara, A. Generalized PT symmetry and real spectra. *J. Phys. A Math. Gen.* **35**, L467 (2002).
17. El-Ganainy, R. et al. Non-Hermitian physics and PT symmetry. *Nat. Phys.* **14**, 11–19 (2018).
18. Guo, A. et al. Observation of PT-symmetry breaking in complex optical potentials. *Phys. Rev. Lett.* **103**, 093902 (2009).
19. Rüter, C. E. et al. Observation of parity–time symmetry in optics. *Nat. Phys.* **6**, 192–195 (2010).

20. Regensburger, A. et al. Parity–time synthetic photonic lattices. *Nature* **488**, 167–171 (2012).
21. Miri, M. A. & Alù, A. Exceptional points in optics and photonics. *Science* **363**, eaar7709 (2019).
22. Leefmans, C. et al. Topological dissipation in a time-multiplexed photonic resonator network. *Nat. Phys.* **18**, 442–449 (2022).
23. Kremer, M. et al. Demonstration of a two-dimensional PT-symmetric crystal. *Nat. Commun.* **10**, 435 (2019).
24. El-Ganainy, R., Makris, K. G., Christodoulides, D. N. & Musslimani, Z. H. Theory of coupled optical PT-symmetric structures. *Opt. Lett.* **32**, 2632–2634 (2007).
25. Kawabata, K., Shiozaki, K., Ueda, M. & Sato, M. Symmetry and topology in non-Hermitian physics. *Phys. Rev. X.* **9**, 041015 (2018).
26. Bandres, M. A. et al. Topological insulator laser: experiments. *Science* **359**, eaar4005 (2018).
27. Hu, B. et al. Non-Hermitian topological whispering gallery. *Nature* **597**, 655–659 (2021).
28. Zhao, H. et al. Non-Hermitian topological light steering. *Science* **365**, 1163–1166 (2019).
29. Weidemann, S. et al. Topological funneling of light. *Science* **368**, 311–314 (2020).
30. Su, R. et al. Direct measurement of a non-Hermitian topological invariant in a hybrid light-matter system. *Sci. Adv.* **7**, eabj8905 (2021).
31. Hu, Y. C. & Hughes, T. Absence of topological insulator phases in non-Hermitian *PT*-symmetric Hamiltonians. *Phys. Rev. B* **84**, 153101 (2011).
32. Weimann, S. et al. Topologically protected bound states in photonic parity–time-symmetric crystals. *Nat. Mater.* **16**, 433–438 (2017).
33. Weidemann, S. et al. Topological triple phase transition in non-Hermitian Floquet quasicrystals. *Nature* **601**, 354–359 (2022).
34. Ghatak, A. et al. Observation of non-Hermitian topology and its bulk–edge correspondence in an active mechanical metamaterial. *Proc. Natl Acad. Sci. USA* **117**, 29561–29568 (2020).
35. Stegmaier, A. et al. Topological defect engineering and *PT* symmetry in non-Hermitian electrical circuits. *Phys. Rev. Lett.* **126**, 215302 (2021).
36. Xia, S. et al. Nonlinear tuning of PT symmetry and non-Hermitian topological states. *Science* **372**, 72–76 (2021).
37. Sone, K., Ashida, Y. & Sagawa, T. Exceptional non-Hermitian topological edge mode and its application to active matter. *Nat. Commun.* **11**, 5745 (2020).
38. Yuce, C. P. T. PT symmetric Floquet topological phase. *Eur. Phys. J. D* **69**, 184 (2015).
39. Kawabata, K. & Sato, M. Real spectra in non-Hermitian topological insulators. *Phys. Rev. Res.* **2**, 033391 (2020).
40. Maczewsky, L. J. et al. Fermionic time-reversal symmetry in a photonic topological insulator. *Nat. Mater.* **19**, 855–860 (2020).
41. Kitagawa, T., Berg, E., Rudner, M. & Demler, E. Topological characterization of periodically driven quantum systems. *Phys. Rev. B* **82**, 235114 (2010).
42. Rudner, M. S., Lindner, N. H., Berg, E. & Levin, M. Anomalous edge states and the bulk-edge correspondence for periodically driven two-dimensional systems. *Phys. Rev. X* **3**, 031005 (2014).
43. Maczewsky, L. J., Zeuner, J. M., Nolte, S. & Szameit, A. Observation of photonic anomalous Floquet topological insulators. *Nat. Commun.* **8**, 13756 (2017).
44. Mukherjee, S. et al. Experimental observation of anomalous topological edge modes in a slowly driven photonic lattice. *Nat. Commun.* **8**, 13918 (2017).
45. Christodoulides, D. N., Lederer, F. & Silberberg, Y. Discretizing light behaviour in linear and nonlinear waveguide lattices. *Nature* **474**, 812–823 (2003).
46. Höckendorf, B., Alvermann, A. & Fehske, H. Topological invariants for Floquet-Bloch systems with chiral, time-reversal, or particle-hole symmetry. *Phys. Rev. B* **97**, 045140 (2018).
47. Höckendorf, B., Alvermann, A. & Fehske, H. Non-Hermitian boundary state engineering in anomalous Floquet topological insulators. *Phys. Rev. Lett.* **123**, 190403 (2019).
48. Szameit, A. & Nolte, S. Discrete optics in femtosecond-laser written photonic structures. *J. Phys. B* **43**, 163001 (2010).
49. Ornigotti, M. & Szameit, A. Quasi *PT*-symmetry in passive photonic lattices. *J. Opt.* **16**, 065501 (2014).
50. Noh, J. et al. Experimental observation of optical Weyl points and Fermi arc-like surface states. *Nat. Phys.* **13**, 611–617 (2017).
51. Peng, Y.-G. et al. Experimental demonstration of anomalous Floquet topological insulator for sound. *Nat. Commun.* **7**, 13368 (2016).
52. Lee, C. H. et al. Topolectrical circuits. *Commun. Phys.* **1**, 39 (2018).

Methods

Wave guide fabrication and sample characterization

We inscribed our coupled wave guide systems with the femtosecond laser direct writing technique[48]. To this end, ultrashort laser pulses of 270 fs duration from a frequency-doubled fibre laser system (Coherent Monaco) at a wavelength of 517 nm and a repetition rate of 333 kHz were focused into a 150 mm × 25 mm × 1 mm fused silica chip (Corning 7980) by means of a microscope objective (×50, numerical aperture = 0.6). The sample was positioned with 50 nm precision by a three-axis motorized translation stage (Aerotech ALS180).

The PT-symmetric Floquet driving protocol was implemented in lattices composed of 4 × 3 unit cells in the x–y plane, for a total of 48 wave guides, and two full Floquet cycles along the propagation direction z. The individual single-mode wave guides are elliptical with a vertical diameter of 7 μm, a horizontal diameter of 2.5 μm and a peak refractive index contrast of 1.7×10^{-3} above the pristine host material's value of 1.46. In our fully passive implementation, non-Hermiticity was implemented by introducing 100 scattering centres[23] in each lossy section, amounting to an intensity attenuation of $(17.7 \pm 0.4)\%$ as calibrated by wave guide fluorescence imaging and fine-tuned by quantitatively evaluating the input-dependent intensity output distributions of specifically designed laser-written non-Hermitian beam splitters. The scattering points were realized by exposing the desired positions to the writing laser for an additional 1.5 s, resulting in microscopic disruptions of the previously inscribed wave guide that scatter light away from it. A micrograph of the lossy coupler region is shown in Supplementary Fig. 2. The desired intra- and inter-sublattice couplings of the driving protocol were realized for wave guide separations of 11.2 μm (resulting in an intensity transfer of $(98.0 \pm 2)\%$ in steps 1, 3, 4 and 6) as well as 9.8 μm and 12.4 μm (resulting in an intensity transfer of $(66.8 \pm 0.5)\%$ and $-(68.8 \pm 0.6)\%$ for steps 2 and 5, respectively). The lattices were characterized by injecting light at 633 nm from a continuous-wave helium–neon laser into specific lattice sites via a microscope objective (×10, numerical aperture = 0.2) and observing the resulting intensity distributions at the sample end facet with a CCD (charge-coupled device) camera (Basler ace).

The recorded output images were evaluated by extracting the relative intensities contained in each wave guide of the lattice, allowing for the calculation of the EOR (that is, the fraction of the overall intensity contained in the lattice sites belonging to the topological edge channels). Similarly, the chirality of the transport arising from single-edge-site excitations was calculated as the ratio between the five leading versus trailing edge sites relative to the point of injection.

Reporting summary

Further information on research design is available in the Nature Portfolio Reporting Summary linked to this article.

Data availability

Source data are provided with this paper. All other data that support results in this Article are available from the corresponding authors upon reasonable request.

Code availability

The codes used to generate the plots within this paper and other findings of this study can be accessed from the corresponding authors upon reasonable request.

Author contributions

A.F., L.J.M. and Y.N.J. developed the theoretical model. A.F., L.J.M., T.B., M.E. and K.B. fabricated the samples and carried out the measurements. A.F. conducted the numerical simulations. A.F. and M.H. evaluated the data and interpreted the results. R.T. and A.S. supervised the efforts of their respective groups. All authors jointly cowrote the manuscript.

Competing interests

The authors declare no competing interests.

Additional information

Supplementary information The online version contains supplementary material available at https://doi.org/10.1038/s41563-023-01773-0.

Correspondence and requests for materials should be addressed to Yogesh N. Joglekar or Alexander Szameit.

Peer review information *Nature Materials* thanks the anonymous reviewers for their contribution to the peer review of this work.

Reprints and permissions information is available at www.nature.com/reprints.

nature portfolio

Corresponding author(s): Alexander Szameit

Last updated by author(s): Nov 2, 2023

Reporting Summary

Nature Portfolio wishes to improve the reproducibility of the work that we publish. This form provides structure for consistency and transparency in reporting. For further information on Nature Portfolio policies, see our Editorial Policies and the Editorial Policy Checklist.

Statistics

For all statistical analyses, confirm that the following items are present in the figure legend, table legend, main text, or Methods section.

n/a	Confirmed	
☐	☒	The exact sample size (*n*) for each experimental group/condition, given as a discrete number and unit of measurement
☐	☒	A statement on whether measurements were taken from distinct samples or whether the same sample was measured repeatedly
☒	☐	The statistical test(s) used AND whether they are one- or two-sided *Only common tests should be described solely by name; describe more complex techniques in the Methods section.*
☒	☐	A description of all covariates tested
☒	☐	A description of any assumptions or corrections, such as tests of normality and adjustment for multiple comparisons
☐	☒	A full description of the statistical parameters including central tendency (e.g. means) or other basic estimates (e.g. regression coefficient) AND variation (e.g. standard deviation) or associated estimates of uncertainty (e.g. confidence intervals)
☒	☐	For null hypothesis testing, the test statistic (e.g. *F*, *t*, *r*) with confidence intervals, effect sizes, degrees of freedom and *P* value noted *Give P values as exact values whenever suitable.*
☒	☐	For Bayesian analysis, information on the choice of priors and Markov chain Monte Carlo settings
☒	☐	For hierarchical and complex designs, identification of the appropriate level for tests and full reporting of outcomes
☒	☐	Estimates of effect sizes (e.g. Cohen's *d*, Pearson's *r*), indicating how they were calculated

Our web collection on statistics for biologists contains articles on many of the points above.

Software and code

Policy information about availability of computer code

Data collection	*Provide a description of all commercial, open source and custom code used to collect the data in this study, specifying the version used OR state that no software was used.*
Data analysis	*Provide a description of all commercial, open source and custom code used to analyse the data in this study, specifying the version used OR state that no software was used.*

For manuscripts utilizing custom algorithms or software that are central to the research but not yet described in published literature, software must be made available to editors and reviewers. We strongly encourage code deposition in a community repository (e.g. GitHub). See the Nature Portfolio guidelines for submitting code & software for further information.

Data

Policy information about availability of data

All manuscripts must include a data availability statement. This statement should provide the following information, where applicable:

- Accession codes, unique identifiers, or web links for publicly available datasets
- A description of any restrictions on data availability
- For clinical datasets or third party data, please ensure that the statement adheres to our policy

The data represented in Figs. 3b and 4 are provided with the paper as source data. All other data that support results in this Article are available from the corresponding author upon reasonable request.

Human research participants

Policy information about [studies involving human research participants and Sex and Gender in Research.](#)

Reporting on sex and gender	*Use the terms sex (biological attribute) and gender (shaped by social and cultural circumstances) carefully in order to avoid confusing both terms. Indicate if findings apply to only one sex or gender; describe whether sex and gender were considered in study design whether sex and/or gender was determined based on self-reporting or assigned and methods used. Provide in the source data disaggregated sex and gender data where this information has been collected, and consent has been obtained for sharing of individual-level data; provide overall numbers in this Reporting Summary. Please state if this information has not been collected. Report sex- and gender-based analyses where performed, justify reasons for lack of sex- and gender-based analysis.*
Population characteristics	*Describe the covariate-relevant population characteristics of the human research participants (e.g. age, genotypic information, past and current diagnosis and treatment categories). If you filled out the behavioural & social sciences study design questions and have nothing to add here, write "See above."*
Recruitment	*Describe how participants were recruited. Outline any potential self-selection bias or other biases that may be present and how these are likely to impact results.*
Ethics oversight	*Identify the organization(s) that approved the study protocol.*

Note that full information on the approval of the study protocol must also be provided in the manuscript.

Field-specific reporting

Please select the one below that is the best fit for your research. If you are not sure, read the appropriate sections before making your selection.

☐ Life sciences   ☐ Behavioural & social sciences   ☐ Ecological, evolutionary & environmental sciences

For a reference copy of the document with all sections, see [nature.com/documents/nr-reporting-summary-flat.pdf](#)

Life sciences study design

All studies must disclose on these points even when the disclosure is negative.

Sample size	*Describe how sample size was determined, detailing any statistical methods used to predetermine sample size OR if no sample-size calculation was performed, describe how sample sizes were chosen and provide a rationale for why these sample sizes are sufficient.*
Data exclusions	*Describe any data exclusions. If no data were excluded from the analyses, state so OR if data were excluded, describe the exclusions and the rationale behind them, indicating whether exclusion criteria were pre-established.*
Replication	*Describe the measures taken to verify the reproducibility of the experimental findings. If all attempts at replication were successful, confirm this OR if there are any findings that were not replicated or cannot be reproduced, note this and describe why.*
Randomization	*Describe how samples/organisms/participants were allocated into experimental groups. If allocation was not random, describe how covariates were controlled OR if this is not relevant to your study, explain why.*
Blinding	*Describe whether the investigators were blinded to group allocation during data collection and/or analysis. If blinding was not possible, describe why OR explain why blinding was not relevant to your study.*

Behavioural & social sciences study design

All studies must disclose on these points even when the disclosure is negative.

Study description	*Briefly describe the study type including whether data are quantitative, qualitative, or mixed-methods (e.g. qualitative cross-sectional, quantitative experimental, mixed-methods case study).*
Research sample	*State the research sample (e.g. Harvard university undergraduates, villagers in rural India) and provide relevant demographic information (e.g. age, sex) and indicate whether the sample is representative. Provide a rationale for the study sample chosen. For studies involving existing datasets, please describe the dataset and source.*
Sampling strategy	*Describe the sampling procedure (e.g. random, snowball, stratified, convenience). Describe the statistical methods that were used to predetermine sample size OR if no sample-size calculation was performed, describe how sample sizes were chosen and provide a rationale for why these sample sizes are sufficient. For qualitative data, please indicate whether data saturation was considered, and what criteria were used to decide that no further sampling was needed.*

Data collection	Provide details about the data collection procedure, including the instruments or devices used to record the data (e.g. pen and paper, computer, eye tracker, video or audio equipment) whether anyone was present besides the participant(s) and the researcher, and whether the researcher was blind to experimental condition and/or the study hypothesis during data collection.
Timing	Indicate the start and stop dates of data collection. If there is a gap between collection periods, state the dates for each sample cohort.
Data exclusions	If no data were excluded from the analyses, state so OR if data were excluded, provide the exact number of exclusions and the rationale behind them, indicating whether exclusion criteria were pre-established.
Non-participation	State how many participants dropped out/declined participation and the reason(s) given OR provide response rate OR state that no participants dropped out/declined participation.
Randomization	If participants were not allocated into experimental groups, state so OR describe how participants were allocated to groups, and if allocation was not random, describe how covariates were controlled.

Ecological, evolutionary & environmental sciences study design

All studies must disclose on these points even when the disclosure is negative.

Study description	Briefly describe the study. For quantitative data include treatment factors and interactions, design structure (e.g. factorial, nested, hierarchical), nature and number of experimental units and replicates.
Research sample	Describe the research sample (e.g. a group of tagged Passer domesticus, all Stenocereus thurberi within Organ Pipe Cactus National Monument), and provide a rationale for the sample choice. When relevant, describe the organism taxa, source, sex, age range and any manipulations. State what population the sample is meant to represent when applicable. For studies involving existing datasets, describe the data and its source.
Sampling strategy	Note the sampling procedure. Describe the statistical methods that were used to predetermine sample size OR if no sample-size calculation was performed, describe how sample sizes were chosen and provide a rationale for why these sample sizes are sufficient.
Data collection	Describe the data collection procedure, including who recorded the data and how.
Timing and spatial scale	Indicate the start and stop dates of data collection, noting the frequency and periodicity of sampling and providing a rationale for these choices. If there is a gap between collection periods, state the dates for each sample cohort. Specify the spatial scale from which the data are taken
Data exclusions	If no data were excluded from the analyses, state so OR if data were excluded, describe the exclusions and the rationale behind them, indicating whether exclusion criteria were pre-established.
Reproducibility	Describe the measures taken to verify the reproducibility of experimental findings. For each experiment, note whether any attempts to repeat the experiment failed OR state that all attempts to repeat the experiment were successful.
Randomization	Describe how samples/organisms/participants were allocated into groups. If allocation was not random, describe how covariates were controlled. If this is not relevant to your study, explain why.
Blinding	Describe the extent of blinding used during data acquisition and analysis. If blinding was not possible, describe why OR explain why blinding was not relevant to your study.

Did the study involve field work? ☐ Yes ☐ No

Field work, collection and transport

Field conditions	Describe the study conditions for field work, providing relevant parameters (e.g. temperature, rainfall).
Location	State the location of the sampling or experiment, providing relevant parameters (e.g. latitude and longitude, elevation, water depth).
Access & import/export	Describe the efforts you have made to access habitats and to collect and import/export your samples in a responsible manner and in compliance with local, national and international laws, noting any permits that were obtained (give the name of the issuing authority, the date of issue, and any identifying information).
Disturbance	Describe any disturbance caused by the study and how it was minimized.

Reporting for specific materials, systems and methods

We require information from authors about some types of materials, experimental systems and methods used in many studies. Here, indicate whether each material, system or method listed is relevant to your study. If you are not sure if a list item applies to your research, read the appropriate section before selecting a response.

Materials & experimental systems

n/a	Involved in the study
☐	☐ Antibodies
☐	☐ Eukaryotic cell lines
☐	☐ Palaeontology and archaeology
☐	☐ Animals and other organisms
☐	☐ Clinical data
☐	☐ Dual use research of concern

Methods

n/a	Involved in the study
☐	☐ ChIP-seq
☐	☐ Flow cytometry
☐	☐ MRI-based neuroimaging

Antibodies

Antibodies used	*Describe all antibodies used in the study; as applicable, provide supplier name, catalog number, clone name, and lot number.*
Validation	*Describe the validation of each primary antibody for the species and application, noting any validation statements on the manufacturer's website, relevant citations, antibody profiles in online databases, or data provided in the manuscript.*

Eukaryotic cell lines

Policy information about cell lines and Sex and Gender in Research

Cell line source(s)	*State the source of each cell line used and the sex of all primary cell lines and cells derived from human participants or vertebrate models.*
Authentication	*Describe the authentication procedures for each cell line used OR declare that none of the cell lines used were authenticated.*
Mycoplasma contamination	*Confirm that all cell lines tested negative for mycoplasma contamination OR describe the results of the testing for mycoplasma contamination OR declare that the cell lines were not tested for mycoplasma contamination.*
Commonly misidentified lines (See ICLAC register)	*Name any commonly misidentified cell lines used in the study and provide a rationale for their use.*

Palaeontology and Archaeology

Specimen provenance	*Provide provenance information for specimens and describe permits that were obtained for the work (including the name of the issuing authority, the date of issue, and any identifying information). Permits should encompass collection and, where applicable, export.*
Specimen deposition	*Indicate where the specimens have been deposited to permit free access by other researchers.*
Dating methods	*If new dates are provided, describe how they were obtained (e.g. collection, storage, sample pretreatment and measurement), where they were obtained (i.e. lab name), the calibration program and the protocol for quality assurance OR state that no new dates are provided.*

☐ Tick this box to confirm that the raw and calibrated dates are available in the paper or in Supplementary Information.

Ethics oversight	*Identify the organization(s) that approved or provided guidance on the study protocol, OR state that no ethical approval or guidance was required and explain why not.*

Note that full information on the approval of the study protocol must also be provided in the manuscript.

Animals and other research organisms

Policy information about studies involving animals; ARRIVE guidelines recommended for reporting animal research, and Sex and Gender in Research

Laboratory animals	*For laboratory animals, report species, strain and age OR state that the study did not involve laboratory animals.*

Wild animals	Provide details on animals observed in or captured in the field; report species and age where possible. Describe how animals were caught and transported and what happened to captive animals after the study (if killed, explain why and describe method; if released, say where and when) OR state that the study did not involve wild animals.
Reporting on sex	Indicate if findings apply to only one sex; describe whether sex was considered in study design, methods used for assigning sex. Provide data disaggregated for sex where this information has been collected in the source data as appropriate; provide overall numbers in this Reporting Summary. Please state if this information has not been collected. Report sex-based analyses where performed, justify reasons for lack of sex-based analysis.
Field-collected samples	For laboratory work with field-collected samples, describe all relevant parameters such as housing, maintenance, temperature, photoperiod and end-of-experiment protocol OR state that the study did not involve samples collected from the field.
Ethics oversight	Identify the organization(s) that approved or provided guidance on the study protocol, OR state that no ethical approval or guidance was required and explain why not.

Note that full information on the approval of the study protocol must also be provided in the manuscript.

Clinical data

Policy information about clinical studies

All manuscripts should comply with the ICMJE guidelines for publication of clinical research and a completed CONSORT checklist must be included with all submissions.

Clinical trial registration	Provide the trial registration number from ClinicalTrials.gov or an equivalent agency.
Study protocol	Note where the full trial protocol can be accessed OR if not available, explain why.
Data collection	Describe the settings and locales of data collection, noting the time periods of recruitment and data collection.
Outcomes	Describe how you pre-defined primary and secondary outcome measures and how you assessed these measures.

Dual use research of concern

Policy information about dual use research of concern

Hazards

Could the accidental, deliberate or reckless misuse of agents or technologies generated in the work, or the application of information presented in the manuscript, pose a threat to:

No | Yes

☐ ☐ Public health

☐ ☐ National security

☐ ☐ Crops and/or livestock

☐ ☐ Ecosystems

☐ ☐ Any other significant area

Experiments of concern

Does the work involve any of these experiments of concern:

No | Yes

☐ ☐ Demonstrate how to render a vaccine ineffective

☐ ☐ Confer resistance to therapeutically useful antibiotics or antiviral agents

☐ ☐ Enhance the virulence of a pathogen or render a nonpathogen virulent

☐ ☐ Increase transmissibility of a pathogen

☐ ☐ Alter the host range of a pathogen

☐ ☐ Enable evasion of diagnostic/detection modalities

☐ ☐ Enable the weaponization of a biological agent or toxin

☐ ☐ Any other potentially harmful combination of experiments and agents

ChIP-seq

Data deposition

☐ Confirm that both raw and final processed data have been deposited in a public database such as GEO.

☐ Confirm that you have deposited or provided access to graph files (e.g. BED files) for the called peaks.

Data access links *May remain private before publication.*	*For "Initial submission" or "Revised version" documents, provide reviewer access links. For your "Final submission" document, provide a link to the deposited data.*
Files in database submission	*Provide a list of all files available in the database submission.*
Genome browser session (e.g. UCSC)	*Provide a link to an anonymized genome browser session for "Initial submission" and "Revised version" documents only, to enable peer review. Write "no longer applicable" for "Final submission" documents.*

Methodology

Replicates	*Describe the experimental replicates, specifying number, type and replicate agreement.*
Sequencing depth	*Describe the sequencing depth for each experiment, providing the total number of reads, uniquely mapped reads, length of reads and whether they were paired- or single-end.*
Antibodies	*Describe the antibodies used for the ChIP-seq experiments; as applicable, provide supplier name, catalog number, clone name, and lot number.*
Peak calling parameters	*Specify the command line program and parameters used for read mapping and peak calling, including the ChIP, control and index files used.*
Data quality	*Describe the methods used to ensure data quality in full detail, including how many peaks are at FDR 5% and above 5-fold enrichment.*
Software	*Describe the software used to collect and analyze the ChIP-seq data. For custom code that has been deposited into a community repository, provide accession details.*

Flow Cytometry

Plots

Confirm that:

☐ The axis labels state the marker and fluorochrome used (e.g. CD4-FITC).

☐ The axis scales are clearly visible. Include numbers along axes only for bottom left plot of group (a 'group' is an analysis of identical markers).

☐ All plots are contour plots with outliers or pseudocolor plots.

☐ A numerical value for number of cells or percentage (with statistics) is provided.

Methodology

Sample preparation	*Describe the sample preparation, detailing the biological source of the cells and any tissue processing steps used.*
Instrument	*Identify the instrument used for data collection, specifying make and model number.*
Software	*Describe the software used to collect and analyze the flow cytometry data. For custom code that has been deposited into a community repository, provide accession details.*
Cell population abundance	*Describe the abundance of the relevant cell populations within post-sort fractions, providing details on the purity of the samples and how it was determined.*
Gating strategy	*Describe the gating strategy used for all relevant experiments, specifying the preliminary FSC/SSC gates of the starting cell population, indicating where boundaries between "positive" and "negative" staining cell populations are defined.*

☐ Tick this box to confirm that a figure exemplifying the gating strategy is provided in the Supplementary Information.

Magnetic resonance imaging

Experimental design

Design type	*Indicate task or resting state; event-related or block design.*

Design specifications	*Specify the number of blocks, trials or experimental units per session and/or subject, and specify the length of each trial or block (if trials are blocked) and interval between trials.*
Behavioral performance measures	*State number and/or type of variables recorded (e.g. correct button press, response time) and what statistics were used to establish that the subjects were performing the task as expected (e.g. mean, range, and/or standard deviation across subjects).*

Acquisition

Imaging type(s)	*Specify: functional, structural, diffusion, perfusion.*
Field strength	*Specify in Tesla*
Sequence & imaging parameters	*Specify the pulse sequence type (gradient echo, spin echo, etc.), imaging type (EPI, spiral, etc.), field of view, matrix size, slice thickness, orientation and TE/TR/flip angle.*
Area of acquisition	*State whether a whole brain scan was used OR define the area of acquisition, describing how the region was determined.*

Diffusion MRI ☐ Used ☐ Not used

Preprocessing

Preprocessing software	*Provide detail on software version and revision number and on specific parameters (model/functions, brain extraction, segmentation, smoothing kernel size, etc.).*
Normalization	*If data were normalized/standardized, describe the approach(es): specify linear or non-linear and define image types used for transformation OR indicate that data were not normalized and explain rationale for lack of normalization.*
Normalization template	*Describe the template used for normalization/transformation, specifying subject space or group standardized space (e.g. original Talairach, MNI305, ICBM152) OR indicate that the data were not normalized.*
Noise and artifact removal	*Describe your procedure(s) for artifact and structured noise removal, specifying motion parameters, tissue signals and physiological signals (heart rate, respiration).*
Volume censoring	*Define your software and/or method and criteria for volume censoring, and state the extent of such censoring.*

Statistical modeling & inference

Model type and settings	*Specify type (mass univariate, multivariate, RSA, predictive, etc.) and describe essential details of the model at the first and second levels (e.g. fixed, random or mixed effects; drift or auto-correlation).*
Effect(s) tested	*Define precise effect in terms of the task or stimulus conditions instead of psychological concepts and indicate whether ANOVA or factorial designs were used.*

Specify type of analysis: ☐ Whole brain ☐ ROI-based ☐ Both

Statistic type for inference (See Eklund et al. 2016)	*Specify voxel-wise or cluster-wise and report all relevant parameters for cluster-wise methods.*
Correction	*Describe the type of correction and how it is obtained for multiple comparisons (e.g. FWE, FDR, permutation or Monte Carlo).*

Models & analysis

n/a	Involved in the study
☐	☐ Functional and/or effective connectivity
☐	☐ Graph analysis
☐	☐ Multivariate modeling or predictive analysis

Functional and/or effective connectivity	*Report the measures of dependence used and the model details (e.g. Pearson correlation, partial correlation, mutual information).*
Graph analysis	*Report the dependent variable and connectivity measure, specifying weighted graph or binarized graph, subject- or group-level, and the global and/or node summaries used (e.g. clustering coefficient, efficiency, etc.).*
Multivariate modeling and predictive analysis	*Specify independent variables, features extraction and dimension reduction, model, training and evaluation metrics.*